Adaptor protein XB130 is a Rac-controlled component of lamellipodia that regulates cell motility and invasion

Monika Lodyga[1,2,3], Xiao-hui Bai[1], András Kapus[2,3,4,*] and Mingyao Liu[1,3,4,*]

[1]Toronto General Research Institute, University Health Network, Toronto, Ontario, M5G 1L7, Canada
[2]Keenan Research Centre in the Li Ka Shing Knowledge Institute, St. Michael's Hospital, Toronto, Ontario M5B 1W8, Canada
[3]Institute of Medical Sciences, University of Toronto, Ontario M5G 1X8, Canada
[4]Department of Surgery, University of Toronto, Ontario M5G 1X8, Canada
*Authors for correspondence (kapusa@smh.toronto.on.ca; mingyao.liu@utoronto.ca)

Accepted 11 August 2010
Journal of Cell Science 123, 4156-4169
© 2010. Published by The Company of Biologists Ltd
doi:10.1242/jcs.071050

Summary

XB130 is a newly described cytosolic adaptor protein and tyrosine kinase substrate, involved in Src- and RET/PTC-dependent signaling. Although XB130 has been cloned as a homologue of actin-filament-associated protein (AFAP-110), its potential regulation by the actin skeleton and its putative roles in cytoskeleton regulation have not been addressed. Here, we show that XB130 (in contrast to AFAP-110) exhibited robust translocation to the cell periphery in response to various stimuli (including epidermal growth factor, wounding and expression of constitutively active Rac) that elicit lamellipodium formation. In stimulated cells, XB130 localized to the lamellipodial F-actin meshwork. Genetic and pharmacological data suggest that the key trigger for XB130 recruitment is the formation of the branched F-actin itself. Structure-function analysis revealed that both the XB130 N-terminus (167 amino acids) and C-terminus (63 amino acids) harbor crucial regions for its translocation to lamellipodia, whereas the PH domains and Src-targeted tyrosines are dispensable. Importantly, in TPC1 thyroid papillary carcinoma cells, silencing endogenous XB130 decreased the rate of wound closure, inhibited matrigel invasion, reduced lamellipodial persistence and slowed down spreading. Thus, XB130 is a novel Rac- and cytoskeleton-regulated and cytoskeleton-regulating adaptor protein that exhibits high affinity to lamellipodial (branched) F-actin and impacts motility and invasiveness of tumor cells.

Key words: Actin-binding proteins, AFAP1L2, Cytoskeleton, EGF

Introduction

Dynamic remodeling of the actin cytoskeleton is indispensable for many physiological and pathological cellular functions, including shape determination, migration, invasiveness and cell division. To accommodate these diverse processes, a large number of actin regulatory proteins has evolved that either directly control actin organization as nucleating, severing, capping or crosslinking proteins, and/or function as adaptors that link these structural elements to signaling pathways. One representative of such actin regulators with both structural and adaptor functions is actin-filament-associated protein (AFAP)-110, an actin crosslinker that also acts as an activator and subsequent substrate of various Src family kinases (Flynn et al., 1993). AFAP-110 characteristically associates with stress fibers and as a result of its tyrosine kinase-regulating properties, it has been implicated in mechanotransduction, stress fiber stabilization, focal adhesion formation and podosome dynamics (Dorfleutner et al., 2007; Gatesman et al., 2004; Han et al., 2004; Han et al., 2005; Lodyga et al., 2002; Zhang et al., 2007).

In search for molecular relatives of AFAP-110, we have recently cloned and begun to characterize a protein termed XB130 (also known as AFAP1L2, actin-filament-associated protein-1-like 2), which exhibits 35% sequence homology with AFAP-110 (Emaduddin et al., 2008; Xu et al., 2007). The structure of XB130 is characteristic of an adaptor protein because it contains several protein–protein and lipid–protein interaction motifs. Specifically, the N-terminal region includes potential tyrosine-phosphorylation sites and a proline-rich sequence that might interact with SH2- and SH3-domain-containing proteins, respectively; the middle portion harbors two pleckstrin homology (PH) domains that might target the protein to cellular membranes through interactions with specific phospholipids (Haslam et al., 1993), whereas the C-terminal region contains a coiled-coil domain, which might be involved in protein oligomerization and DNA binding.

Regarding functional properties, XB130, similarly to AFAP-110, has been shown to associate with and activate Src kinases presumably via its SH3-binding domain (Xu et al., 2007). Moreover, XB130 is also a substrate of Src and other tyrosine kinases. Indeed, we have shown that XB130, which is abundantly expressed in thyroid follicular cells, serves as a prime target for the oncogenic tyrosine kinase RET/PTC, the pathogenic factor in papillary carcinoma (Lodyga et al., 2009). RET/PTC-mediated phosphorylation of XB130 (predominantly on Y54) recruits and activates phosphatidylinositol-3-kinase (PI3K), which in turn stimulates the Akt pathway and thereby cell proliferation.

Although these studies have identified XB130 as a tyrosine-kinase-regulated, signal-integrating adaptor molecule involved in oncogenesis, its relationship to the cytoskeleton remained unknown. Despite the fact that it was cloned as a homologue of AFAP-110, neither its regulation by the cytoskeleton nor its impact on cytoskeleton regulation or functions have been clarified. It is noteworthy in this respect that AFAP-110 contains a 17 amino acid stretch that was identified as an actin-binding domain (ABD) based on its homology (33–47%) with known ABDs of other actin-binding proteins such as dystrophin, α-actinin and spectrin (Qian et al., 2000). Interestingly, the corresponding region of XB130 shows much less similarity (13–20%) to these actin-binding consensus sites. Moreover, the intracellular localization of AFAP-

Journal of Cell Science

Journal of Cell Science

110 and XB130 is strikingly different in resting cells: the former associates with stress fibers, whereas the latter shows a finely punctuate cytosolic distribution (Xu et al., 2007). This suggests that their relationship with the cytoskeleton is distinct and they might exhibit largely differing affinities for various supramolecular F-actin structures.

The aim of the present study was to gain insight into the potential cytoskeletal regulation and function of XB130. To address this issue, we first asked whether characteristic cytoskeletal reorganizations induced by soluble stimuli or by various active Rho family GTPases (the master regulators of the cytoskeleton) (Etienne-Manneville and Hall, 2002) provoke specific changes in XB130 localization, and if so, which structural domains are necessary for these effects. Conversely, we also asked whether XB130 might be involved in key cytoskeletal functions such as migration and invasion. Our results show that active Rac GTPase or Rac-activating agents induce robust translocation of XB130 (but not AFAP-110) to lamellipodia, and that both the XB130 N-terminus and C-terminus are indispensable for this effect. Downregulation of XB130 in thyroid carcinoma cells decreases lamellipodial persistence, reduces the efficiency of wound closure and inhibits invasion. Thus our findings implicate XB130 as a Rac-controlled regulator of lamellipodial dynamics and cell motility, which might impact both proliferation and invasiveness during carcinogenesis.

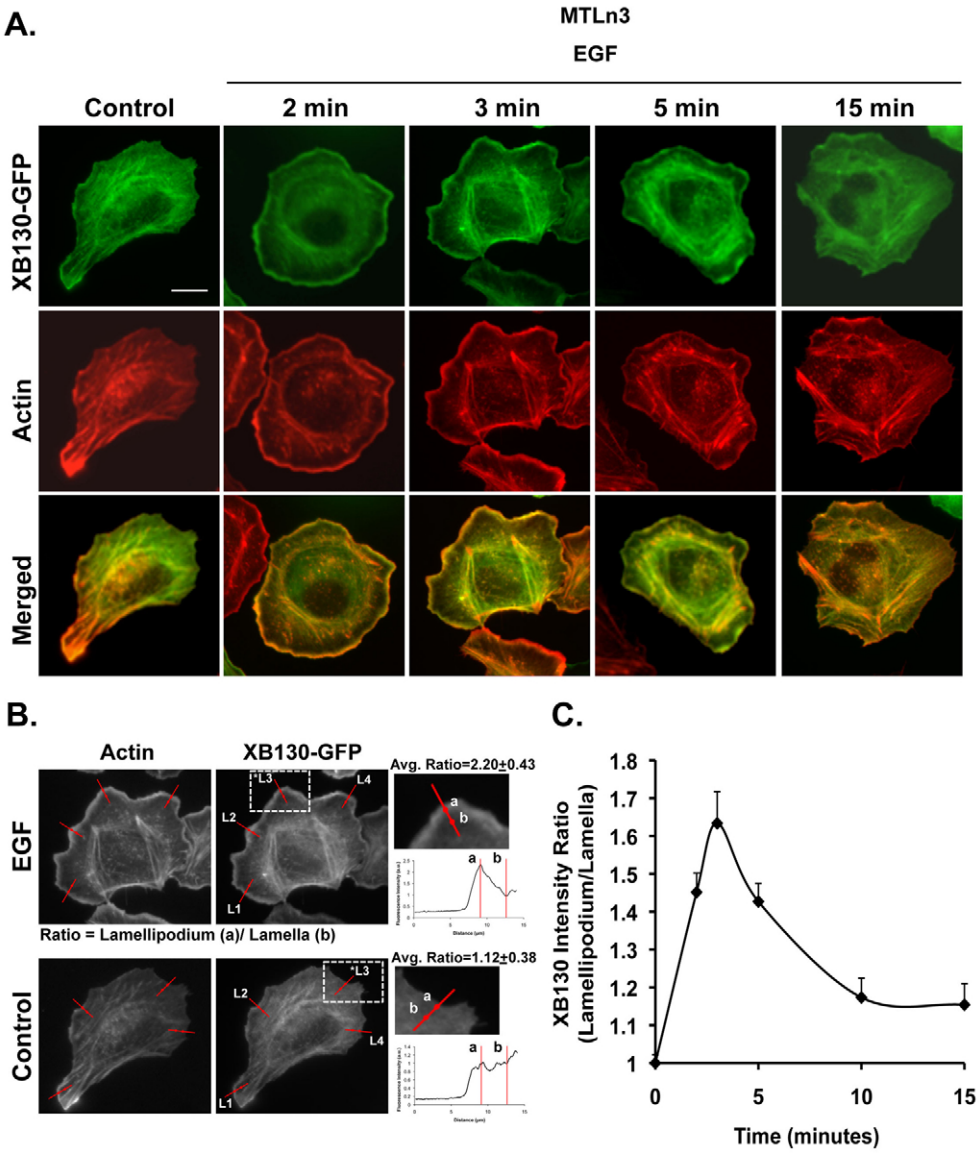

Fig. 1. XB130–GFP accumulates at the cell periphery in response to EGF in MTLn3 cells. (**A**) MTLn3 cells transfected with XB130–GFP were serum-starved for 2 hours before EGF stimulation (5 nM) and fixed at various times. F-actin was labeled with Alexa-Fluor-350–phalloidin (red). Scale bar: 10 µm. Representative images of three similar experiments. (**B**) Quantification of peripheral XB130–GFP accumulation. Four lines were drawn across the lamellipodium (visualized by F-actin) of EGF-stimulated cells. The graph shows the intensity profile along the line marked with an asterisk. The peak intensity in the lamellipodium (a) and the minimal value in the lamella (b) were measured. Four lamellipodium to lamella ratios were determined and averaged for every cell. In case of the unstimulated cells (which are devoid of lamellipodia) this peripheral ratio was determined by measuring fluorescence along similar lines at 2–3 and 5–6 µm from the membrane. (**C**) Time course of peripheral (lamellipodial) accumulation of XB130 after EGF stimulation. Ratios, determined as in B, were normalized to the average of the controls obtained in unstimulated cells. Data are mean ± s.e.m. from >100 different cells. All time points were significantly different from control.

Results

XB130 translocates to the cell periphery concomitant with stimulus-induced cytoskeleton reorganization

To examine whether rapid cytoskeletal remodeling coincides with cellular redistribution of XB130, we expressed GFP-tagged XB130 in MTLn3 rat mammary carcinoma cells, which were then stimulated with epidermal growth factor (EGF) for various times, and fixed and stained with phalloidin. MTLn3 cells represent a particularly suitable model to study the dynamic behavior of cytoskeleton-associated proteins because they respond to EGF with fast, synchronized and robust cytoskeleton reorganization, characterized by an initial phase of large lamellipodial extension, followed by lamellipodial retraction (Chan et al., 1998; Segall et al., 1996). In resting MTLn3 cells, XB130–GFP exhibited a fine punctate distribution, which was restricted to the cytosol (Fig. 1A), in accordance with our earlier findings of endogenous XB130 in other cell types (Xu et al., 2007). EGF rapidly (within 2 minutes) induced the formation of large flat lamellipodia, which contained a continuous belt of F-actin under the plasma membrane (Fig. 1A). Intriguingly, in parallel with the emergence of these active zones of F-actin assembly, XB130 showed marked peripheral accumulation and colocalization with the newly formed F-actin meshwork in a belt-like pattern. Quantification of the XB130–GFP signal showed an increase in accumulation of approximately 1.6-fold (calculated as shown in Fig. 1B) at the leading edge at 3 minutes, followed by a gradual return to near-basal levels by 15 minutes (Fig. 1C).

In the following experiments, we used live video microscopy to concomitantly monitor EGF-induced shape changes and XB130 translocation in single cells, as well as to compare the behavior of XB130–GFP and AFAP-110–GFP (Fig. 2). In agreement with the data obtained on fixed cells, EGF provoked (within 100 seconds) a substantial increase in the cell area as a result of lamellipodial extension, and caused marked translocation of XB130–GFP to the periphery. The peripheral XB130–GFP accumulation peaked at 160–200 seconds and decreased by 260 seconds (Fig. 2A and supplementary material Movie 1). This time course corresponds well with the kinetics of peripheral F-actin assembly as previously reported in the same cell type (Chan et al., 1998; Mouneimne et al., 2004). In addition to the belt-like XB130–GFP accumulation, we often observed dynamic ‘hot spots’ at the edge of the lamellipodium (supplementary material Movie 2) in the form of narrow lines, which tended to move along the periphery and occurred at sites of intense membrane ruffling. The distribution of AFAP-110–GFP was dramatically different. Under basal conditions AFAP-110–GFP was organized in fiber-like patterns and smaller patches, strictly restricted to the central areas of the cell. These structures probably correspond to stress fibers and central focal adhesions, as reported earlier (Zhang et al., 2007). Importantly, EGF stimulation failed to induce peripheral translocation of AFAP-110–GFP during the entire course of the experiments (up to 10 minutes) (supplementary material Movie 3). This was not due to an AFAP-110–GFP expression-induced inhibition of the lamellipodial extension per se, as verified by the ensuing EGF-triggered change in cell area and shape (Fig. 2B). Finally control experiments confirmed that GFP itself showed neither characteristic accumulation under basal conditions, nor peripheral accumulation upon EGF stimulation (Fig. 2C). These findings imply that lamellipodium formation is associated with peripheral accumulation of XB130, but not AFAP-110, suggesting that the two proteins have very different affinities for diverse actin-containing structures.

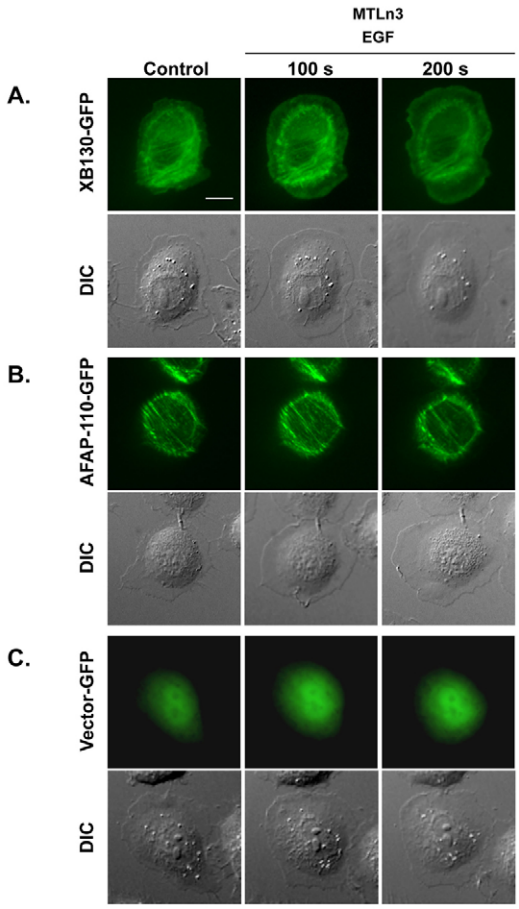

Fig. 2. Differential localization and responsiveness to EGF treatment of XB130 and AFAP-110. Representative micrographs of MTLn3 cells transfected with GFP-tagged XB130 (**A**), AFAP-110 (**B**), or vector control (**C**) were taken using live, time-lapse video microscopy. Twenty-four hours after transfection, MTLn3 cells were serum starved for 2 hours then challenged with 5 nM EGF. Images were collected just before treatment (control) and every 20 seconds following the addition of EGF. DIC and fluorescent images shown were obtained at 100 and 200 seconds. Scale bar: 10 μm.

To validate the phenomenon of stimulus-induced translocation in natural XB130 expressors, we used a thyroid papillary carcinoma cell line (TPC1), which has been shown to express high levels of endogenous XB130 (Lodyga et al., 2009). To provoke lamellipodium formation, TPC1 cells were stimulated with a protein kinase C activator, phorbol-myristate acetate (PMA), a potent inducer of this process. Immunofluorescent labeling using an anti-XB130 antibody revealed that in untreated TPC1 cells XB130 was uniformly distributed in the cytosol. PMA treatment (30 minutes), which triggered the formation of large lamellipodia as visualized with Rhodamine–phalloidin staining, induced strong XB130 accumulation at the edges of these newly formed F-actin-rich protrusions (Fig. 3A) without causing detectable association of XB130 with stress fibers. In addition, XB130 was also recruited to the lamellipodium of TPC1 cells, when cell polarization was induced by scraping a wound into a confluent monolayer (Fig. 3B). Taken together, a variety of stimuli (EGF, PMA and cell wounding) induced translocation of endogenous or heterologously expressed XB130 from the cytosol to the cell periphery, where it

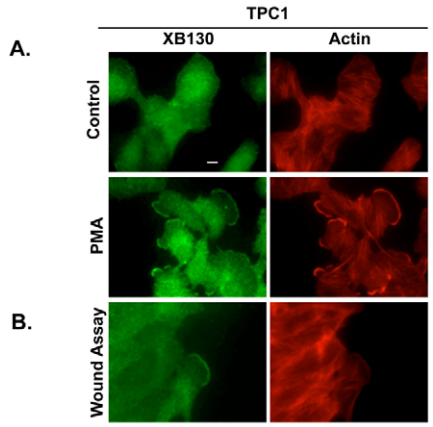

Fig. 3. Endogenous XB130 increases at the leading edge following PMA treatment or wounding. (**A**) TPC1 cells were serum starved and stimulated with 100 nM PMA for 30 minutes, fixed and stained with anti-XB130 antibody and Rhodamine–phalloidin for actin. (**B**) Confluent monolayers of TPC1 cells grown on coverslips were serum starved overnight, and then scratch wounded. The wound healing response was initiated in the presence of FBS enriched medium (20%). After 2 hours, the cells were fixed and stained with anti-XB130 antibody, and Rhodamine-phalloidin for F-actin. Scale bar: 10 µm.

colocalized with the simultaneously formed, membrane-associated actin meshwork.

Effects of Rho GTPases on the cellular distribution of XB130 and AFAP-110

Having observed that soluble stimuli induced XB130 translocation concomitant with cytoskeleton remodeling, we tested the effect of direct and distinct modes of cytoskeleton modification on XB130 distribution. To this end we transfected natural expressors of XB130, WRO cells (thyroid follicular carcinoma cells), with either constitutively active (CA) forms of GFP–RhoA(Q63L) or Rac1(Q61L), two members of the Rho GTPase family that are known to induce various F-actin structures, namely stress fibers and lamellipodia, respectively. For a control, the WRO cells were transfected with empty GFP vector and subsequently all groups underwent immunofluorescent staining to label XB130 and F-actin. Presence of the GFP vector did not produce visible changes in XB130 distribution compared with surrounding untransfected cells (Fig. 4A). Importantly, although CA-Rho induced strong stress fiber formation, there was no major colocalization of XB130 with these structures. By contrast, CA-Rac, which caused dissolution of central stress fibers and formation of dorsal ruffles and lamellipodia, induced XB130 translocation to the latter structures (Fig. 4A).

To compare the distribution of XB130 and AFAP-110, we transfected MTLn3 cells with XB130–GFP or AFAP-110–GFP along with the Myc-tagged, constitutively active form of Rac(Q61L) and stained for the expressed small GTPase (Myc) and F-actin. CA-Rac induced a lamellipodium formation along the entire periphery, and robust accumulation of XB130 at the same site (Fig. 4B), similarly to that observed upon EGF treatment. Beside this predominant effect, XB130 was also distributed along fine, internal fibers. AFAP-110 showed a very different response. AFAP-110 overexpression itself tended to increase the number of stress fibers. CA-Rac, when coexpressed with AFAP-110, induced not only a peripheral actin belt, but it also enhanced the formation

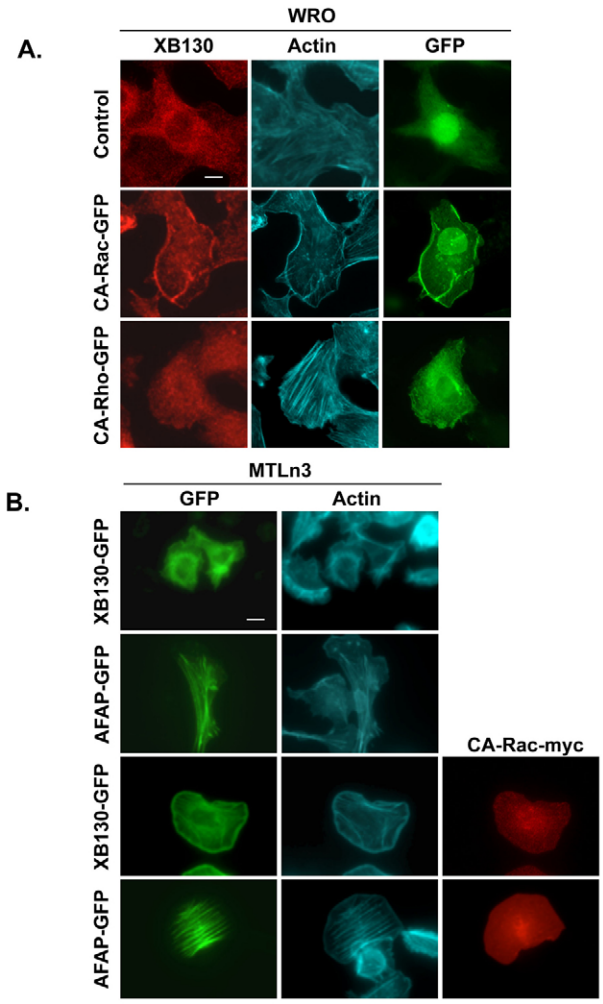

Fig. 4. Active Rac induces the translocation of XB130 to the cell periphery. (**A**) WRO cells were transfected with plasmids encoding either empty GFP vector, CA-Rac–GFP or CA-Rho–GFP. Twenty-four hours after transfection cells were fixed and stained with monoclonal anti-XB130 antibody and Alexa-Fluor-350–phalloidin for F-actin. (**B**) MTLn3 cells were transfected with GFP-tagged XB130 or AFAP-110 alone or in combination with Myc-tagged CA-Rac(Q61L). Twenty-four hours after transfection they were fixed and stained with anti-Myc antibody to visualize CA-Rac and Alexa-Fluor-350–phalloidin. Note the dramatic colocalization of XB130 and F-actin in the CA-Rac-induced peripheral F-actin belt, and the colocalization between F-actin stress fibers and AFAP-110. Scale bars: 10 µm.

of central stress fibers. Remarkably, although CA-Rac strongly promoted AFAP-110 accumulation in these central fibers, it did not induce any peripheral translocation to the lamellipodia. Thus, AFAP-110 facilitates the formation of stress fibers, and shows high affinity to these structures, whereas it does not associate with Rac-induced peripheral F-actin networks.

Taken together, our results indicate that active Rac induced robust peripheral translocation of XB130 in a pattern that was identical with that observed after exposure to external stimuli (Fig. 1A, Fig. 2A and Fig. 3). Because Rac promotes the formation of a highly branched F-actin meshwork under the membrane, and XB130 colocalizes with the Rac-triggered F-actin belt, these results suggest that XB130 has a high affinity to and predominantly associates with structures that contain branched F-actin.

Journal of Cell Science

Cellular redistribution of XB130 to the periphery is dependent upon the actin meshwork

We sought to determine if the formation of the actin meshwork per se is critical for the peripheral recruitment of XB130. To this end we co-transfected GFP tagged XB130 with dominant negative Rac (T17A) (Takaishi et al., 1994). As expected, DN-Rac completely prevented the EGF-induced formation of the F-actin belt. Instead, in the absence of Rac activity EGF provoked the formation of thin filopodial extensions (Fig. 5A). Importantly, DN-Rac (concomitant with the inhibition of lamellipodium formation) entirely prevented the peripheral (submembranous) accumulation of XB130. Under these conditions XB130 remained predominantly cytoplasmic or showed mild accumulation at the base of the filopodial projections (Fig. 5A).

To substantiate that the relocalization of XB130 is concomitant with and presumably due to the assembly of the branched F-actin network, we used Cytochalasin D (CytoD), which prevents the incorporation of new actin monomers into polymers by blocking the barbed ends (MacLean-Fletcher and Pollard, 1980). CytoD abolished the formation of the EGF-induced actin belt and prevented the peripheral translocation of XB130. In the presence of CytoD GFP-tagged XB130 formed punctate clumps throughout the cytoplasm, in both resting and in EGF-challenged cells (Fig. 5B). These findings further support the notion that actin assembly itself (as opposed to membrane lipid changes or other factors) is the key trigger that targets XB130 to the cell periphery.

Finally, we asked whether F-actin assembly is not only necessary but also sufficient to provoke XB130 translocation, even in the absence of specific signaling events. To address this we treated MTLn3 cells with Jasplakinolide (JK), a sponge toxin that is a potent and direct inducer of de novo actin nucleation (Bubb et al., 2000). JK triggered the formation of thick cytosolic F-actin conglomerates, as shown earlier (Bubb et al., 2000; Fan et al., 2004). These showed strong colocalization with cytosolic clumps of XB130 (Fig. 5C). Taken together, these data show that the assembly of F-actin structures have a key role in the translocation of XB130 to the cell periphery.

The presence of the N-terminal and C-terminal domain is required for translocation of XB130 to the lamellipodia

The following experiments were conducted to discern which domains or regions of XB130 are crucial for its Rac-dependent peripheral translocation. XB130 contains a variety of domains that in principle might contribute to its peripheral (membrane and/or lamellipodial) redistribution (Fig. 6A). Key candidate regions included the two pleckstrin homology domains, PH1 (aa 175–271) and PH2 (aa 353–446), which might be involved in the interaction between proteins and membrane phospholipids; the so called unique region (aa 491–648), which holds the lowest amino acid sequence homology to AFAP-110; the coiled-coiled motif (aa 652–750), which shows similarity to a region in AFAP-110 that harbors a leucine zipper motif for protein–protein interaction and a 17-residue stretch that is essential for F-actin binding or cross-linking; the N-terminus (aa 2–169), which contains SH3- and SH2-domain binding motifs, several tyrosine kinase target residues (e.g. Y54), as well as a putative actin-binding motif (see the Discussion); and the C-terminus (aa 757–817), which again shows little similarity to AFAP-110.

To address the involvement of these molecular regions, we generated a set of GFP- and Myc-tagged truncation (Δ) mutants lacking one or more of the above-mentioned sequences as well as the Y54F point mutant (Fig. 6A, Fig. 7A). These Myc- or GFP-tagged XB130 constructs were then cotransfected into MTLn3 cells with GFP- or

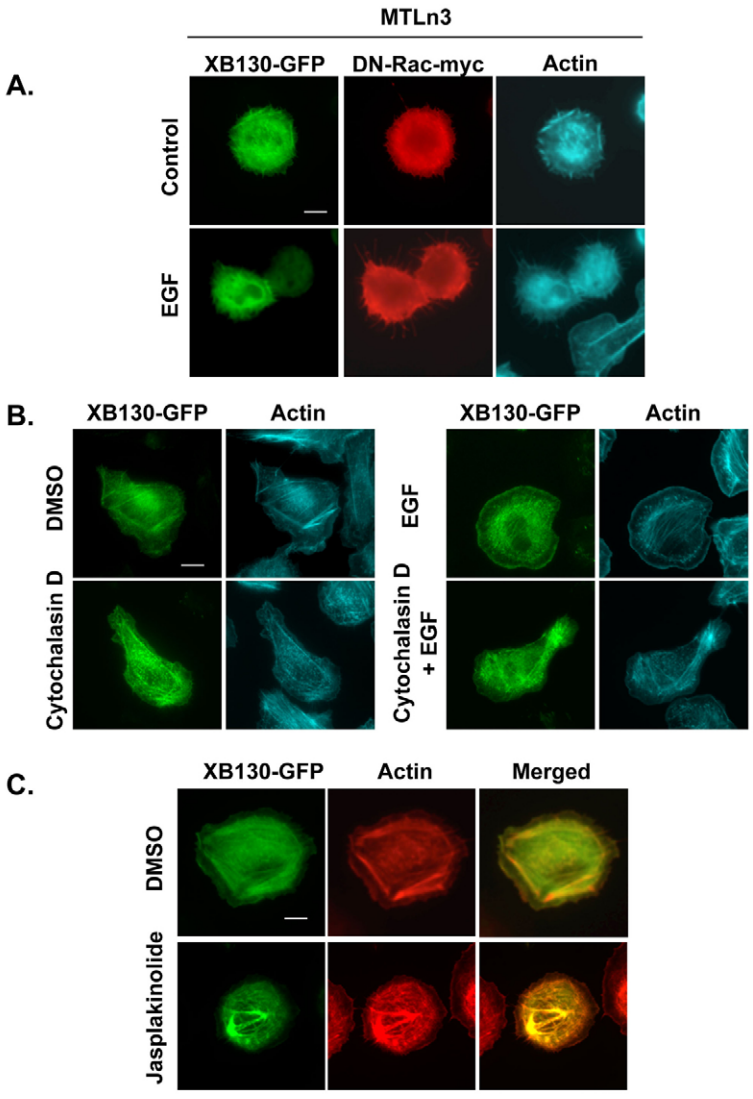

Fig. 5. Formation of the F-actin meshwork at the cell periphery is a prerequisite for XB130 translocation. (**A**) DN-Rac prevents the EGF-induced formation of the submembranous actin belt and the peripheral translocation of XB130. MTLn3 cells were co-transfected with GFP–XB130 and DN-Rac–Myc, left untreated or stimulated with EGF for 3 minutes, and then fixed and stained with Alexa-Fluor-350–phalloidin and Myc antibody (DN-Rac). (**B**) Cytochalasin D eliminates EGF-induced XB130 translocation. Cells were transfected with XB130–GFP pretreated with DMSO or 100 nM Cytochalasin D for 1 minute, followed by EGF stimulation for 3 minutes, and then processed as above. (**C**) Pharmacologically induced F-actin polymerization is sufficient to redistribute XB130–GFP into F-actin clusters. XB130–GFP transfected MTLn3 cells were treated with 100 nM Jasplakinolide for 30 minutes. Subsequently, cells were fixed and stained with Alexa-Fluor-350–phalloidin (red). Scale bars: 10 μm.

Journal of Cell Science

Myc-tagged CA-Rac (respectively), and the cells were analyzed by double or triple immunofluorescent labeling to visualize the distribution of XB130, CA-Rac and F-actin. The latter staining was used to distinguish the potential effect of a given construct on the Rac-induced cytoskeleton remodeling per se, as opposed to the construct's ability to translocate to the periphery. We performed these experiments in MTLn3 cells to avoid confounding effects that could be created by the presence of endogenous XB130 protein in natural expressors such as protein dimerization or dominant-negative effects. The Myc-labeled XB130 mutants were used to ensure that any observed lack of translocation was not simply due to an interference of the bulky GFP tag with the movement of the truncated XB130. The results were quantified with two complementary methods: we determined the percentage of the cells with peripheral XB130, as well measured the ratio of the peripheral versus central XB130 fluorescence in a set of single cells, expressing the various mutants. Using these approaches, our results can be summarized as follows: deletion of the PH domains, either individually or in combination, had no effect on CA-Rac-induced XB130 translocation (Fig. 6). These constructs accumulated in a peripheral belt similarly to the wild type, implying that membrane phospholipid–XB130 interactions do not have a significant role in the translocation. Similarly, deletion of the unique region (ΔUR) or the coiled-coiled domain (Δ coiled-coiled) did not prevent XB130 recruitment to the periphery, because obvious translocation occurred in 80% of the transfected cells (Fig. 7B). Nonetheless, the extent of accumulation for both mutants at the cell periphery was significantly reduced (Fig. 7C), suggesting that these regions, although not indispensable, might contribute to the efficiency of XB130 recruitment or retention in the lamellipodia. By contrast, deletion of the N-terminus led to a dramatic reduction (70–80%) in peripheral recruitment when assessed either by cell percentage or the lamellipodium to lamella ratio (Fig. 7B,C; see Fig. 1B) Moreover, Tyr54, which is the main target for Src and Ret/PTC kinases located in the N-terminus, was not involved in the translocation, because its replacement with phenylalanine did not alter the process. Deletion of the C-terminus also robustly (75–80%) inhibited the CA-Rac-triggered redistribution (Fig. 7B,C). This mutant also seemed to have lost its capacity to localize to central fibers (Fig. 7A). The combined deletion of the N- and the C-terminus essentially abolished peripheral translocation (Fig. 7A–C). It is noteworthy that in the presence of these mutants (ΔN, ΔC, ΔN&C), the CA-Rac-induced formation of the lamellipodial F-actin belt was not affected or only marginally reduced, implying that these mutants indeed have diminished affinity to this structure. Identical observations were made with Myc- or GFP-tagged mutants (Fig. 7D). Finally, we tested the responsiveness of these XB130 mutant proteins using a natural, external stimulus, EGF. In agreement with the above data, deletion of either the N- or the C-terminus alone or in combination, caused a pronounced translocation defect, whereas deletions of other regions (ΔUR, Δcoiled-coil) or the Y54F mutation failed to markedly affect cellular redistribution (Fig. 8A,B). We next examined whether the N-terminal region (the first 167 aa) or the C-terminal region (the last 63 aa) of XB130 was sufficient for targeted translocation to lamellipodia (Fig. 9A). In resting cells the GFP-

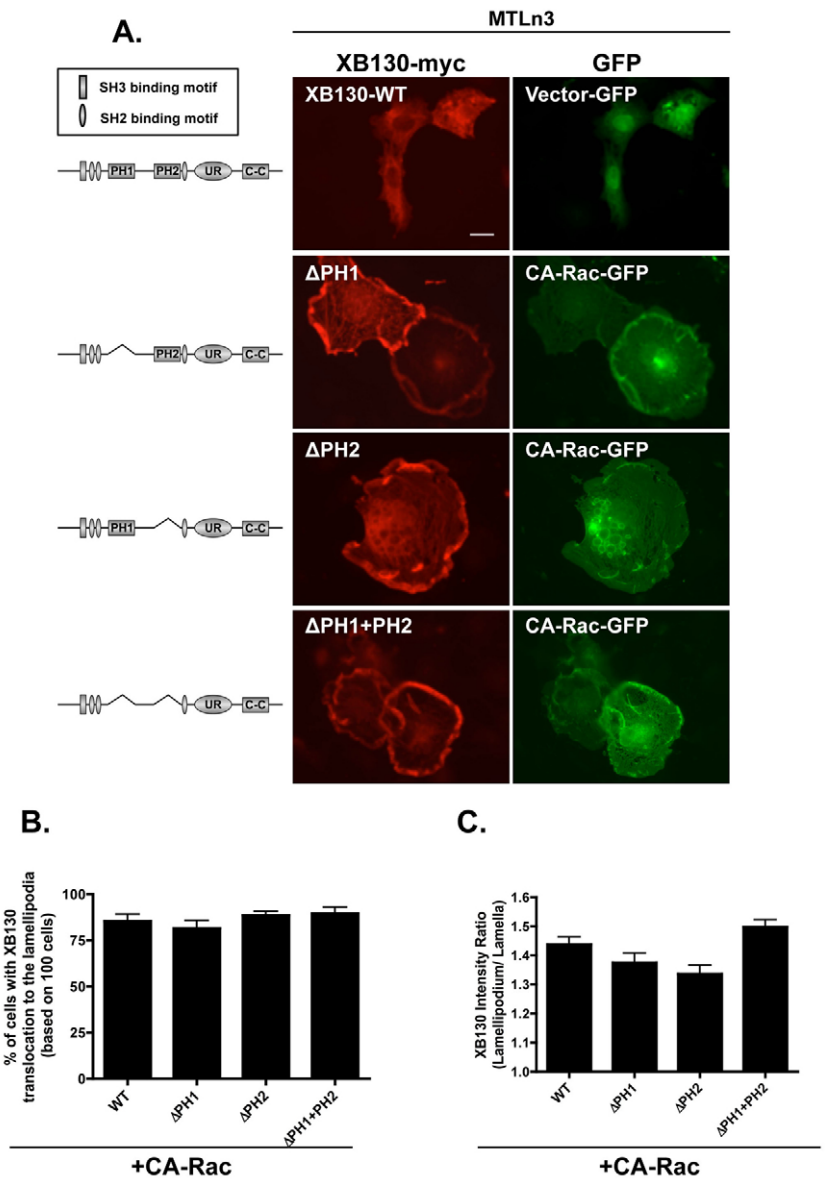

Fig. 6. Deletion of PH domains, either individually or in combination, had no effect on the CA-Rac- induced XB130 translocation. (**A**) Schematic representation of XB130 protein and deletion mutants; PH, pleckstrin homology domain; UR, unique region; C-C, coiled-coil domain. MTLn3 cells were transfected with various Myc-tagged PH-domain deletion XB130 constructs along with CA-Rac(Q61L)–GFP, fixed 24 hours after transfection and immunostained with anti-Myc antibody for XB130. Scale bar: 10 µm. (**B**) Quantification of data shown in A; the values were derived by assessing the lamellipodial accumulation of XB130 in 100 doubly transfected cells. (**C**) Quantification of fluorescence intensity of the XB130 signal at the lamellipod as normalized to the region just below the lamellipod as performed in Fig. 1B. Data are the mean ± s.e.m. from 40 cells.

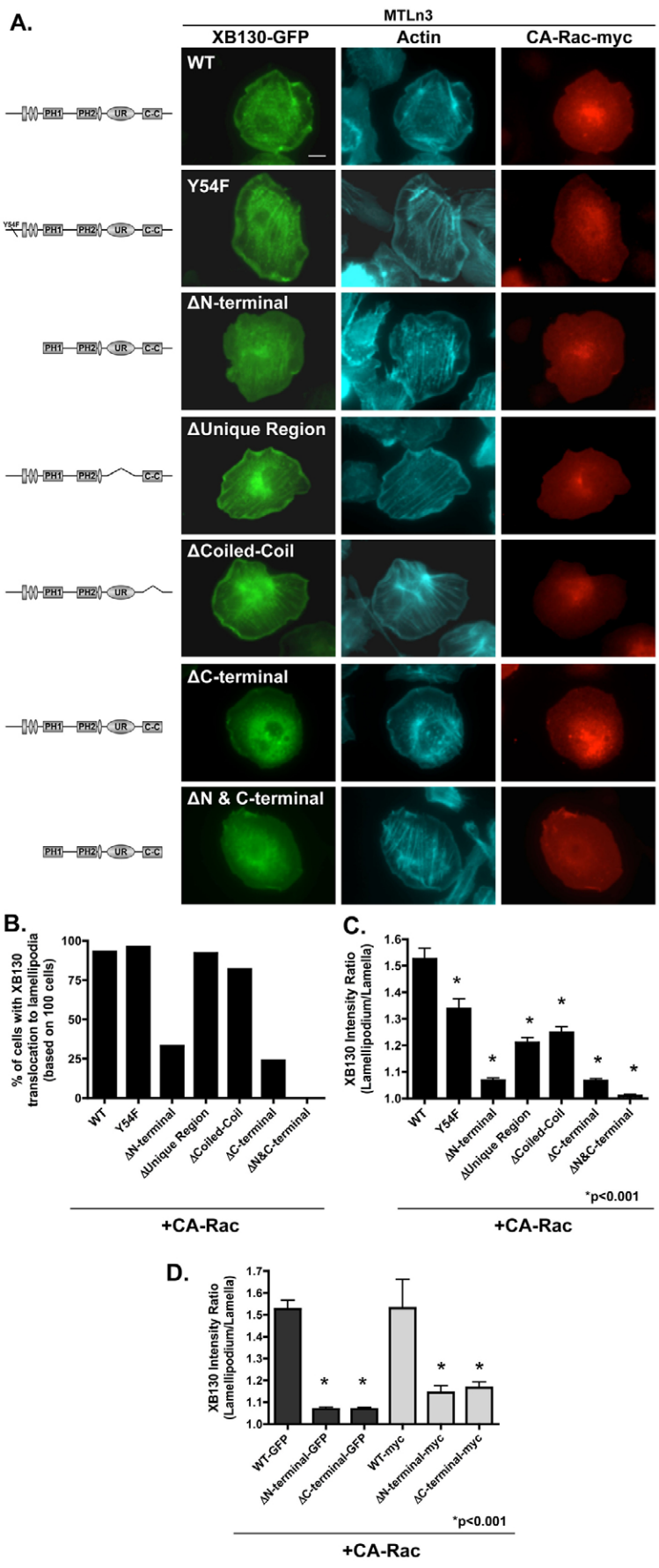

tagged N167 aa construct, showed cytoplasmic localization with some enrichment in the perinuclear area (Fig. 9B), whereas the C63 aa construct, although predominantly cytoplasmic, also exhibited some nuclear localization (Fig. 9C). Both constructs were distributed to the periphery by CA-Rac or EGF treatment, although the responses were less robust than in the case of the full-length XB130 (Fig. 9B,C). Taken together, these data show that both the N- and the C-terminal regions have an important role in the translocation and cytoskeletal association of XB130.

XB130 contributes to cell migration and invasiveness

Having shown that XB130 translocates to lamellipodia, we asked whether it could have an impact on typical lamellipodial functions, such as cell migration and invasion. To this end, we targeted XB130 (*AFAP1L2*) mRNA in TPC1 cells using two distinct short interfering RNAs (siRNAs). When combined, they caused >90% knockdown of XB130 (Fig. 10A). To assess the effect of XB130 downregulation on cell movement, we used a wound-closure assay. XB130-depleted cells exhibited significantly reduced migration into the denuded area compared with the non-related siRNA-treated controls (Fig. 10B,D). After 12 hours, the gap remaining between the wound edges was nearly twofold wider in the XB130-downregulated culture than in the control (54% vs 29%, when normalized to the original width of 100%) (Fig. 10C).

Since directional tumor cell migration often occurs across a matrix (basement membrane) along a chemoattractant gradient in a three-dimensional context, we next modeled this process, using a Matrigel invasion assay. Control or XB130-depleted TPC1 cells were placed onto Matrigel-coated Transwell inserts in a 3D migration chamber, with serum-enriched medium in the lower compartment. The number of invading cells was quantified 24 hours after seeding. There was a significant reduction in the invasive capacity of the XB130-knockdown group compared with the control, as visualized by the Crystal-Violet-stained inserts (Fig. 11A) and quantified by microscopy (Fig. 11B).

Next, we asked whether XB130 might affect lamellipodial dynamics, an effect that might underlie the observed defects in migration and invasion. To address

Fig. 7. Both the N-terminal and the C-terminal regions contribute to the Rac-dependent translocation of XB130 to the lamellipodia. (**A**) Schematic representation of XB130 protein and deletion mutants. MTLn3 cells were transfected with various XB130 deletion constructs along with CA-Rac(Q61L)–Myc, fixed 24 hours after transfection and immunostained with anti-Myc antibody for CA-Rac, as well as Alexa-Fluor-350–phalloidin for actin. Scale bar: 10 μm. (**B**) Quantification of data shown in B; the values were derived as in Fig. 1B. (**C**) Quantification of fluorescence intensity of the GFP signal at the lamellipod as in Fig. 6C. Data are the mean ± s.e.m. from 70 cells. (**D**) Comparison of the distribution of Myc- vs GFP-tagged XB130 constructs; Quantification was performed as in Fig. 1B. Data are the mean ± s.e.m. from 60 cells. Note that the behavior of the differentially labeled constructs is identical. **P*<0.001 compared with WT.

Journal of Cell Science

this, control or XB130-downregulated TPC1 cells were treated with PMA for 30 and 60 minutes, and then fixed and stained for F-actin. We then quantified the number of cells with lamellipodia in each group based on the appearance of linear F-actin deposition at the cell periphery. Every cell that had at least one lamellipodium was counted as positive (Fig. 12A,B). Only a few untreated cells possessed lamellipodia, and no significant difference was seen in the number of such cells between control and XB130-depleted cultures. After a 30 minute exposure to PMA, the number of cells with lamellipodium showed a similar increase in both groups. However, after a 60 minute stimulation, a significantly smaller portion of cells possessed lamellipodia in the XB130-knockdown group than in the control (≈30% difference, $P<0.001$) (Fig. 12C). This result suggests that although XB130 is not required for early lamellipodium formation, it appears to contribute to lamellipodial persistence in thyroid cells.

Finally, we tested whether the absence of XB130 impacts cell spreading, another function related to lamellipodial dynamics and edge protrusion. To address this, control and XB130-downregulated cells were trypsinized, re-plated onto glass coverslips, washed and fixed after various times. Spreading was quantified by measuring the area covered by individual cells (see representative images in Fig. 13A). The average cell area was significantly lower at each time point in XB130-downregulated cells than in the corresponding controls (>150 cells per each time and condition) (Fig. 13B). The rate of spreading (normalized to the size attained after attachment at 15 minutes) was a ≈30% less for the XB130-downregulated cells than for the controls, implying that XB130 contributes to efficient edge protrusion.

Taken together, these experiments show that downregulation of XB130 decreased lamellipodial persistence, reduced the rate of wound closure, inhibited invasion and slowed down cell spreading,

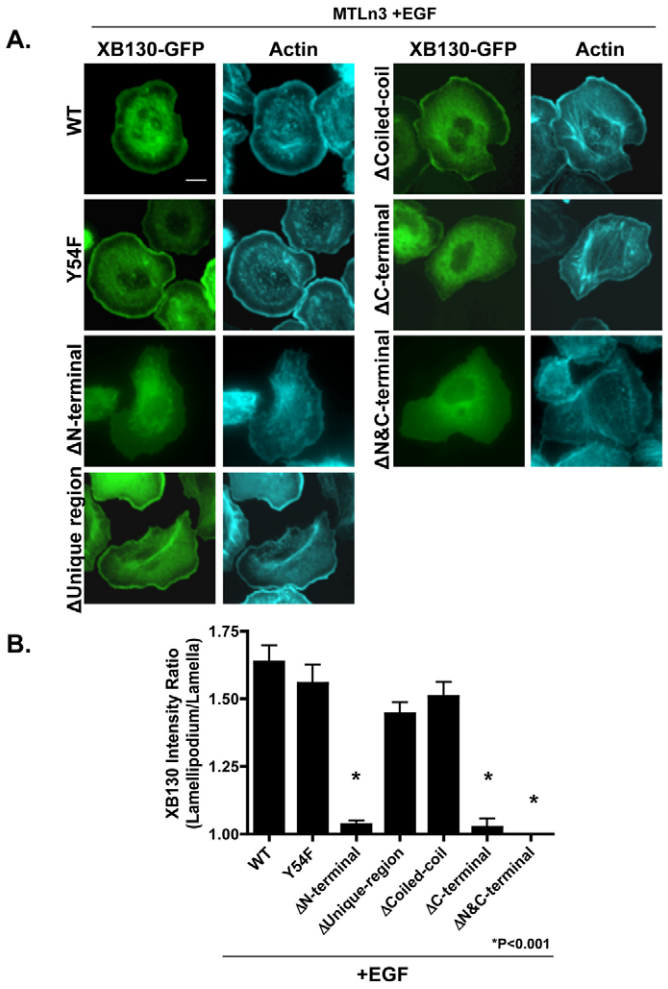

Fig. 8. Deletion of the N- and C-terminal region impairs the ability of XB130 to accumulate at the lamellipodia in response to EGF stimulation. (**A**) MTLn3 cells were transfected with various XB130 deletion constructs, serum starved and stimulated for 3 minutes with EGF (5 nM). Cells were fixed and stained with Alexa-Fluor-350–phalloidin for actin. Scale bar: 10 µm. (**B**) Quantification of fluorescence intensity of the GFP signal at the lamellipod as normalized to the region just below the lamellipod (lamella) and to the average ratio of unstimulated cells. Data are the mean ± s.e.m. from 70 cells. *$P<0.001$ compared with WT.

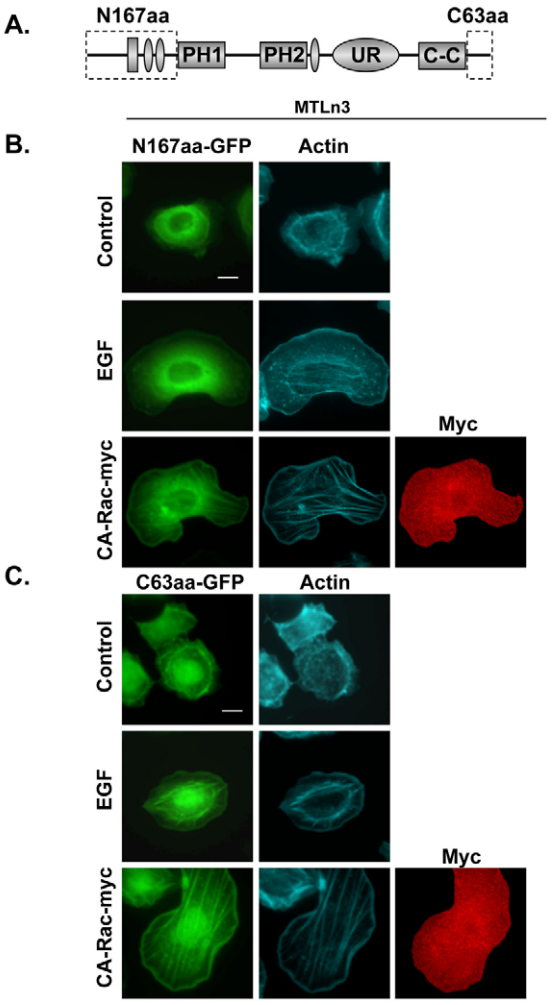

Fig. 9. N167aa and C63aa sequences of XB130 are sufficient for EGF or CA-Rac-induced XB130 translocation to cell periphery. (**A**) A 167 amino acid region of the XB130 N-terminus as well as a 63 amino acid region of the C-terminus was amplified and placed into a GFP construct. (**B**) GFP-tagged N167 construct and (**C**) C63 construct were transfected into MTLn3 cells alone or together with CA-Rac–Myc. Cells were fixed 24 hours after transfection and stained for actin with Alexa-Fluor-350–phalloidin. For EGF treatment, cells were starved and stimulated with EGF (5 nM) for 5 minutes. Scale bars: 10 µm.

Journal of Cell Science

supporting the concept that XB130 contributes to the regulation of actin dynamics and cell motility.

Discussion

XB130 has been recently cloned by our group as a molecular homologue of AFAP-110 (Xu et al., 2007). Although the regulation and potential functions of this protein have just begun to be elucidated, it has already emerged as a unique and functionally multifaceted adaptor molecule. Our previous studies have demonstrated that XB130 shows an organ-specific expression pattern (e.g. highly enriched in the thyroid epithelium), and has an important role in the regulation of cell survival and proliferation as a substrate and binding partner of various tyrosine kinases (Src, RET-PTC). Specifically, we found that in thyroid carcinoma cells, tyrosine phosphorylation of XB130 by the oncogenic RET-PTC kinase induces its direct binding to the regulatory subunit of PI3K (p85), which then leads to PI3K-dependent activation of the Akt pathway (Lodyga et al., 2009). These signaling studies, however, have not implicated XB130 as a cytoskeleton-related protein, although its similarity to AFAP-110 has given credence to such a hypothesis. The present work provides evidence that XB130 is regulated by the actin cytoskeleton, and it impacts key cytoskeletal functions, such as cell migration and invasion. These observations reveal a new aspect of the complex biology of XB130.

Generation of specific antibodies against human XB130 enabled us to study the distribution of this protein in natural expressors, such as bronchial alveolar epithelial cells (BEAS-2B) and various thyroid papillary carcinoma lines. These initial investigations revealed that in non-stimulated cells, endogenous XB130 exhibits an even cytosolic distribution, in contrast to AFAP-110, which is organized along F-actin fibers (Flynn et al., 1993). Indeed, simultaneous double staining for these proteins confirmed their distinct distribution within the same cells (Xu et al., 2007). This implies that XB130 has little affinity to crosslinked, central F-actin filaments. Accordingly, association of XB130 with stress fibers was observed only upon heterologous overexpression, and it remained modest even under these conditions. In addition to their distinct localization in resting cells, our current work uncovers the dramatically different responsiveness of these two proteins. Although AFAP-110 failed to show major redistribution upon cellular stimulation, XB130 exhibited robust translocation to the cell periphery, both in endogenous and heterologous expressors. The common denominator in the effect of the applied external and internal stimuli (EGF, PMA, CA-Rac) is that each induces major cytoskeleton remodeling, characterized by actin nucleation and branching-type (Arp2/3-dependent), de novo F-actin assembly under the plasma membrane (Chan et al., 2000; Ichetovkin et al., 2002; Taunton et al., 2000). This process results in the formation of a dense and dynamic submembranous F-actin meshwork that exerts a force upon the plasma membrane, giving rise to the formation of lamellipodia and membrane ruffles. Importantly, these structures are the very sites where XB130 is accumulated in a stimulus-induced fashion. In agreement with the fact that Rac is the major inducer of lamellipodia and ruffles (Nobes and Hall, 1995), this small GTPase has a primary role in the regulation of XB130 distribution. A similar conclusion can be drawn from our

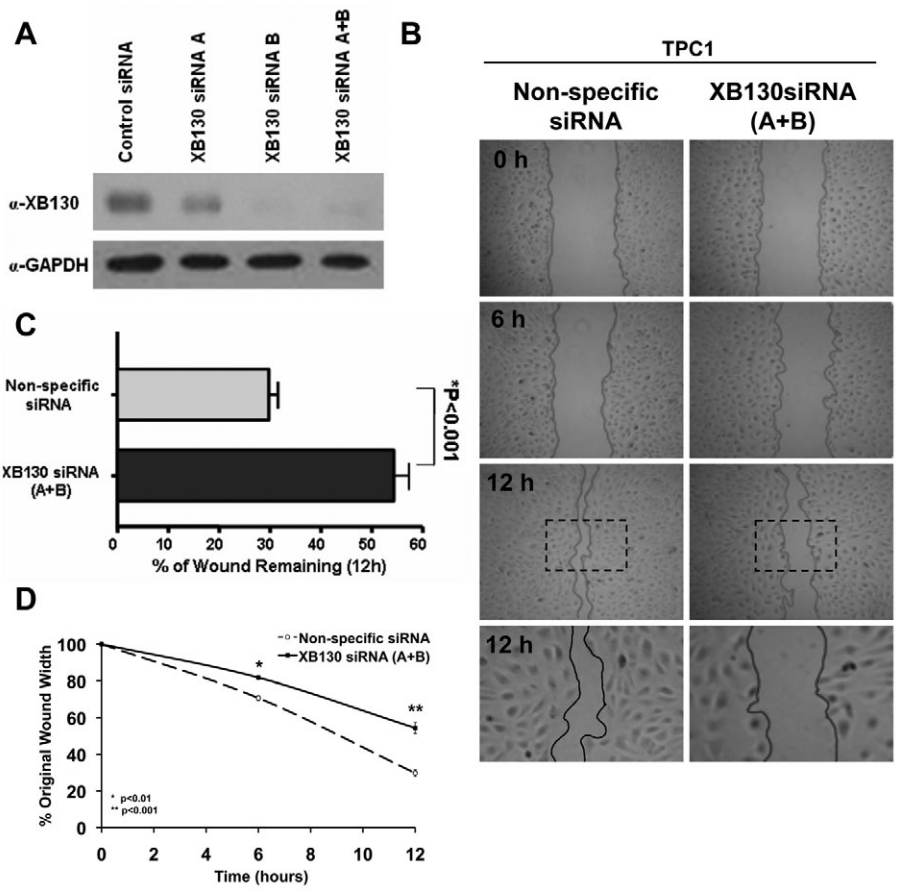

Fig. 10. Knockdown of XB130 suppresses wound closure in TPC1 monolayers. (**A**) TPC1 cells were treated with control siRNA or a mixture of two siRNAs to knock down XB130 (A and B, 75 nM total). The efficiency of the XB130 downregulation was confirmed by western blot using GAPDH as a loading control. (**B**) TPC1 cells were grown to confluence, treated with non-specific siRNA or siRNAs to knock down XB130 (A+B), serum starved overnight, subjected to wounding and treated with FBS-enriched medium (20%) to initiate wound closure. Images were collected at time 0, 6 and 12 hours. Bottom image is an enlargement from area indicated on the 12 hour panel. To quantify the wound closure, measurements were taken of wound width. Data are mean ± s.e.m. from 18 fields per group, per time. (**C**) Histogram representation of wound status in groups treated with the non-specific siRNA and siRNA against XB130 at 12 hours following wound induction. (**D**) Quantification of wound closure progression at time 0, 6 and 12 hours. **P*<0.01 and **P*<0.001 compared with original wound width.

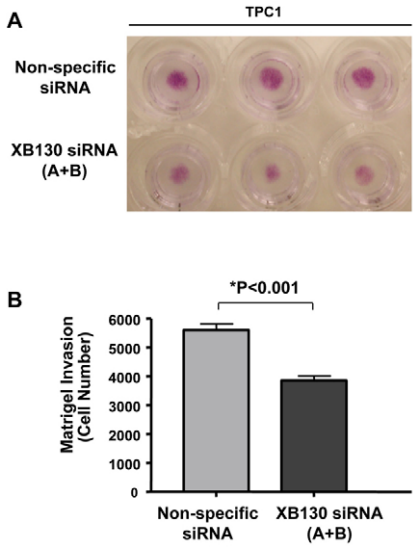

Fig. 11. Downregulation of XB130 decreases Matrigel invasion by TPC1 cells. (**A**) Representative image of Transwell inserts containing Crystal-Violet-stained, transmigrated cells. TPC1 cells were transfected with two specific siRNAs to knock down XB130 (A and B, 75 nM total) or with non-specific siRNA as a control. Twenty-four hours after transfection, cells were trypsinized, counted and seeded onto three-dimensional migration chamber inserts for Matrigel invasion assay. After 24 hours, cells remaining in the top layer were removed, while transmigrated cells were stained with Crystal Violet. (**B**) Matrigel Invasion was quantified using ten random fields per insert (five inserts per group) in a blinded fashion and was normalized for differences in proliferation. Downregulation of XB130 reduced cell invasion (P<0.001), in comparison with non-specific siRNA-treated group.

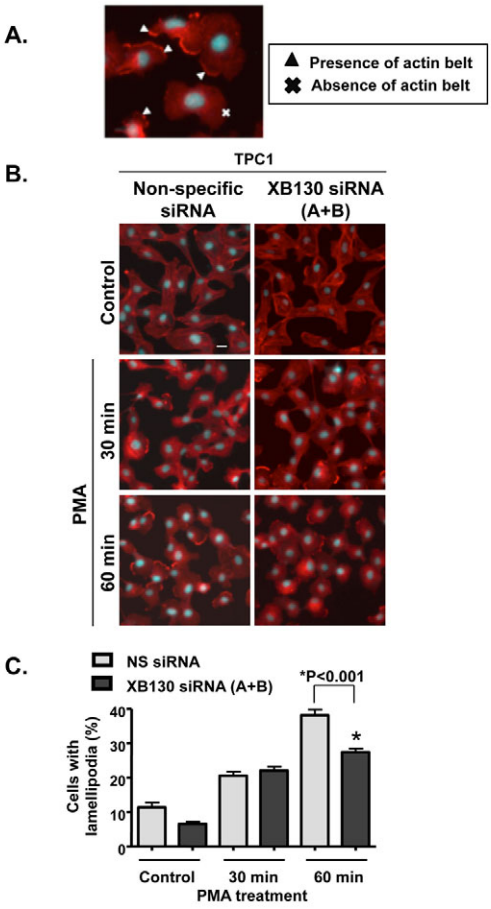

Fig. 12. XB130-knockdown TPC1 cells exhibit reduced lamellipodial persistence. TPC1 cells were transfected with either control siRNA or siRNAs to knock down XB130 (A+B) (75 nM total), starved overnight, stimulated with 100 nM PMA for 30 or 60 minutes fixed and stained with Rhodamine–phalloidin as well as nuclear Hoechst stain. (**A**) The micrographs were scored based on the number of cells that exhibited lamellipodial F-actin accumulation. Positive and negative cells are indicated with arrowheads and cross, respectively. (**B**) Representative images. (**C**) Quantification of data shown in B; the values were obtained from the number of cells with lamellipodia in XB130-knockdown (A+B) and control group. Means + s.e.m. *P<0.001 compared with control siRNA cells.

experiments showing that CA-Rac induced XB130 accumulation in the lamellipodia. Moreover, DN-Rac prevented the stimulus-induced peripheral translocation of XB130, concomitant with the inhibition of lamellipodium formation per se. By contrast, CA-Rho, which induces the assembly of stress fibers (via Rho kinase) and F-actin cables (via formins) (Tominaga et al., 2000) did not have a major impact on XB130 distribution. Furthermore, our observations not only imply that XB130 has particular affinity to branched, or de novo formed F-actin, but also suggest that the actin meshwork per se (or its formation) is an important recruiting factor. This view is supported by the finding that pharmacologically provoked (JK-induced) assembly of F-actin patches attracts XB130 to these clusters and, conversely, inhibition of F-actin assembly (by CytoD) prevents the translocation of XB130. Collectively, these data indicate that AFAP-110 and XB130 possess differing affinities towards actin structures, the former preferring cables, whereas the latter branches. From a functional standpoint, XB130 belongs to those cytoskeletal adapter proteins (such as cortactin) (Weed et al., 1998), which associate with and are markers for ‘hot spots’ of peripheral actin dynamics.

We performed a systematic mutational analysis to gain insight into the structural requirements for peripheral translocation and actin meshwork association of XB130. The fact that both PH domains are dispensable suggests that direct binding to membrane phospholipids is not needed for translocation, and reinforces the view that interaction with peripheral F-actin might be the key mechanism. The crucial F-actin binding domain of AFAP-110 is located close to the leucine zipper region, and shares a consensus sequence with other F-actin binding proteins, including dystrophin, α-actinin and spectrin (Qian et al., 2000). However, the corresponding region of XB130 shows only marginal similarity with these sequences; moreover, deletion of the coiled-coiled domain (which includes this region) failed to affect XB130 translocation and its colocalization with F-actin. By contrast, deletion of either the N-terminus (167 aa) or the C-terminus (63 aa) substantially reduced the stimulus- and CA-Rac-induced translocation of XB130, implying the involvement of distinct and multiple sequences. Conversely, the isolated N- or C-termini could still translocate (albeit exhibiting lesser accumulation than the full-length protein) to the periphery. Intriguingly, we noted that the first 14 amino acids of XB130 share substantial similarity with a distinct type of actin binding domain, classified by Taylor and colleagues (Taylor et al., 1998) as ABD2 (as opposed to ABD1 and ABD3 found in AFAP-110) (supplementary material Fig. S1). Proteins harboring this domain include the membrane-cytoskeleton linker

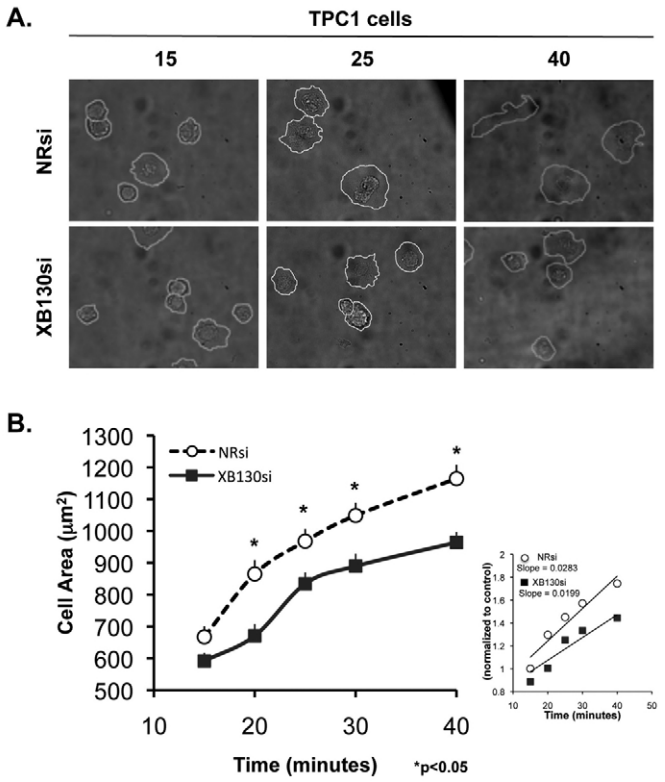

Fig. 13. Downregulation of endogenous XB130 decreases cell spreading. (**A**) TPC1 cells transfected for 48 hours with either control siRNA or siRNAs to knock down XB130 (A+B) were suspended and re-plated onto coverslips. The coverslips were washed and fixed at 15, 20, 25, 30 and 40 minutes intervals. Cell area was assessed by DIC microscopy. Representative images are shown for the selected time points. (**B**) Image analysis was used to quantify the mean area per cell; data are means + s.e.m. obtained from three separate experiments, 150 cells were traced per group. Statistically significant differences (P<0.05) (comparing the areas at corresponding time points) are indicated with an asterisk. To express the rate of spreading (slope in the investigate time frame) data from B was normalized to the area of the control at 15 minutes (graph on right). Note that there is a 30% reduction in the spreading rate.

radixin, the focal adhesion component talin, and the capping protein Capz (Matsui et al., 1998; Turunen et al., 1994). It is therefore conceivable that an ABD2 in the N-terminus of XB130 is a main determinant of its interaction with F-actin structures. Although it awaits direct verification, this proposition is also consistent with the similarities between the distribution and function of these proteins and XB130. Namely, radixin was shown to localize to the leading edge where it contributes to lamellipodial stability (Baumgartner et al., 2006; Castelo and Jay, 1999). Similarly, talin, in addition to its localization in focal adhesions, can also accumulate in lamellipodia (DePasquale and Izzard, 1991), and has important roles in the regulation of edge protrusion and cell motility (Smith et al., 2005).

The N-terminus of XB130 also contains several tyrosine kinase target sites. Since tyrosine phosphorylation of XB130, especially at Tyr54, proved to be crucial for docking and activation of the p85 subunit of PI3K (Lodyga et al., 2009), we investigated whether this process might also be involved in XB130 redistribution. However, we found that (1) the Y54F mutation did not affect the CA-Rac- or EGF-induced XB130 translocation; (2) overexpression of Src (data not shown), a condition that was shown to enhance XB130 tyrosine phosphorylation (Xu et al., 2007) failed to cause translocation; and (3) EGF, which induced robust translocation, did not promote tyrosine phosphorylation of heterologously expressed XB130 in carcinoma cells (data not shown). These observations suggest that XB130 tyrosine phosphorylation is neither necessary nor sufficient for peripheral XB130 translocation. Rather, tyrosine phosphorylation that might follow XB130 translocation could promote the recruitment of signaling molecules (e.g. PI3K) to the peripheral F-actin meshwork.

The structural basis of the affinity of the XB130 C-terminus to F-actin remains to be established. However, it might be noteworthy that the C-terminus appears to be less selective with respect to F-actin organization, because it shows comparable association with stress fibers and lamellipodia. Future studies are warranted to discern whether the N- and C-termini of the intact XB130 interact and form a common F-actin binding site, and/or promote XB130 anchoring via direct and indirect mechanisms, i.e. by binding to F-actin or other lamellipodial proteins, respectively.

In the last part of our studies we sought to gain insight into the functional significance of XB130 as a cytoskeleton-associated protein. For these experiments we used thyroid papillary carcinoma cell lines, which express high levels of XB130. Knockdown of XB130 resulted in slower cell migration in a wound-healing model and diminished matrigel invasion, indicating that XB130 indeed impacts key cytoskeletal functions. Although knockdown of XB130 did not seem to affect lamellipodium formation per se (at least when evoked by PKC stimulation), it significantly reduced lamellipodial persistence. This effect could be one of the mechanisms underlying impaired migration and invasion. Regarding the potential molecular mechanisms whereby XB130 might influence lamellipodial dynamics, it is noteworthy that RET kinase phosphorylation has been shown to activate Rac via PI3K. Specifically, phosphorylation of Y1062 in RET can recruit and activate PI3K, and the subsequently formed phosphatidylinositol-3,4,5-trisphosphate stimulates Rac guanine nucleotide exchange factors (GEFs) (Fukuda et al., 2002). Importantly, our previous studies have shown that, in addition to this direct pathway, oncogenic RET can activate PI3K indirectly, by binding XB130, which in turn interacts with and activates PI3K through Y54 (Lodyga et al., 2009). This scaffolding function proved to be important, because knockdown of XB130 dramatically reduced PI3K-dependent Akt activation in thyroid carcinoma cells (Lodyga et al., 2009). It is therefore conceivable that an initial assembly of branched actin structures recruits XB130, which in turn helps to localize PI3K to these structures. These events might result in a spatially restricted, as well as augmented or prolonged PI3K and Akt activation, which in turn might manifest in more persistent or recurring lamellipodial activity. Both PI3K and Akt are known to promote migration and invasion (Keely et al., 1997; Weiner et al., 2002; Yip et al., 2004). An alternative but non-exclusive possibility evokes the fact that XB130 (similarly to AFAP-110) is not only a substrate, but also an activator of Src kinases (Xu et al., 2007). Thus, XB130 associated with the peripheral cytoskeleton might locally augment the activity of Src kinases, which are well-known regulators of migration and invasion (Huveneers and Danen, 2009). These possibilities are attractive inasmuch that they connect the previously described signaling functions (PI3K/Akt, Src kinase regulation) with the currently described stimulus-induced cytoskeleton-associated distribution of XB130. Future studies should test these possibilities, using natural XB130 expressors and RET-activating stimuli.

Journal of Cell Science

Journal of Cell Science

In summary, we provide evidence that XB130 is a cytoskeleton-regulated and cytoskeleton-regulating adaptor protein that associates with peripheral F-actin in a stimulus-dependent fashion and modifies cell motility and invasiveness.

Materials and Methods

Materials

Human recombinant epidermal growth factor (EGF) was from Austral Biologicals (San Ramon, CA). Phorbol-12-myristate-13-acetate (PMA), DMSO, rat tail type I collagen, soybean trypsin inhibitor, Cytochalasin D (CytoD) and Hoechst 33342 dye were from Sigma (St Louis, MO). Protease inhibitor cocktail was obtained from Pharmingen (San Diego, CA). Jasplakinolide (JK), Rhodamine-phalloidin and Alexa-Fluor-350–phalloidin were purchased from Invitrogen (San Diego, CA). The monoclonal anti-XB130 antibody was described previously (Xu et al., 2007). The following antibodies were purchased: anti-c-myc (9E10) (Santa Cruz Biotechnology, Santa Cruz, CA), GAPDH (Trevigen, Gaithersburg, MD). Peroxidase-conjugated anti-mouse IgG and ECL® kit were obtained from Amersham Biosciences. Cy3-labeled mouse anti-IgG was obtained from Jackson ImmunoResearch Laboratories (West Grove, PA). siRNA duplexes were purchased from Dharmacon (Lafayette, CO).

Cell culture

Rat mammary adenocarcinoma (MTLn3) cells were provided by Jeffrey E. Segall (Albert Einstein College of Medicine, Bronx, NY). The cells were grown in α-minimal essential medium (α-MEM), (Invitrogen), supplemented with 5% (v/v) heat-inactivated fetal bovine serum (FBS) and 1% antibiotic suspension (penicillin–streptomycin, Invitrogen). MTLn3 cells were used between passages 25 and 35 and were subcultured in 60–70% subconfluent conditions. Cells were plated on rat tail type 1 collagen coated coverslips. Thyroid papillary carcinoma cells, TPC1 were provided by Massimo Santoro (Università di Napoli Federico II, Naples Italy), and were grown in Dulbecco's Modified Eagle's medium (DMEM) (Invitrogen), supplemented with 10% FBS and 1% penicillin–streptomycin. WRO cells were provided by Sylvia Asa (University Health Network, Toronto, Ontario, Canada) and were grown in RPMI 1640 supplemented with 10% FBS, 1% penicillin-streptomycin, 1% sodium pyruvate (Invitrogen) and 1% non-essential amino acids (Invitrogen). All cells were cultured in a standard humidified incubator at 37°C in a 5% CO_2 atmosphere and 95% air.

Cell-stimulation conditions

Cells were serum-starved with α-MEM medium supplemented with 0.5% FBS for 2–4 hours (MTLn3) or in DMEM overnight (TPC1) before experiments. Cells were stimulated with 5 nM human recombinant EGF for various times, or 100 nM PMA, as indicated in the figure legends. Where used, Cytochalasin D (100 nM) (or DMSO as control) was added to the cells for 1 minute before addition of EGF. Jasplakinolide was used at 100 nM for 30 minutes. For transient transfections, cells were plated for 24 hours, followed by transfection using FuGene6™ reagent (Roche Molecular Diagnostics, Basel, Switzerland) according to the manufacturer's instructions.

Plasmid construction

N-terminally GFP-tagged XB130 was generated using Myc-tagged XB130 as a template by PCR amplification using PfuTurbo (Stratagene, La Jolla, CA). XB130–GFP forward primer (5′-CGGAATTCTATGGAGCGGTACAAAG-3′) contained *Eco*RI site, whereas the reverse primer (5′-AAACGCGTCGACCTAACTT-GCTCCTT-3′) contained a *Sal*I site. The generated PCR product was subcloned into *Eco*RI–*Sal*I sites of pEGFP-c1. XB130 mutant constructs were generated as follows: GFP-XB130 in pEGFP-c1 or XB130 Myc in the pcDNA3.1myc-HisA backbone was subjected to single or double rounds of site-directed mutagenesis using the QuikChange Site-Directed Mutagenesis kit (Stratagene), according to the manufacturer's recommendations. The primers used are listed in supplementary material Table S1. N-terminal (N167aa) and C-terminal (C63aa) GFP-tagged constructs were obtained by PCR amplification using the primer pairs listed in the supplementary material Table S2. The generated N167aa and C63aa fragments were subcloned into *Eco*RI and *Sal*I sites. All of the constructs were verified by DNA sequencing (The Centre for Applied Genomics, Hospital for Sick Children, Toronto, ON, Canada).

Myc-tagged constructs encoding wild-type human XB130 (XB130-myc) or point mutant in which Tyr54 was replaced by phenylalanine (Y54F) were described previously (Lodyga et al., 2009). The Rho GTPase plasmids were previously described; Rac^{Q61L}–Myc, Rac^{T17N}–Myc (Benard et al., 1999; Chong et al., 1994; Takaishi et al., 1994; Zhang et al., 1995), GFP–Rac^{Q61L}, GFP–Rho^{Q63L} (Subauste et al., 2000). GFP–AFAP-110 construct was a kind gift from Dr Flynn (West Virginia University, Morgantown, WV) (Qian et al., 2000).

Protein studies

Immunoblotting experiments were performed according to standard procedures described previously (Han et al., 2004; Lodyga et al., 2002). Briefly, cells were harvested in lysis buffer (50 mM HEPES, pH 7.5, 150 mM NaCl, 10% glycerol, 1% Triton X-100, 1 mM EGTA, 1.5 mM $MgCl_2$, 10 mM NaF, 10 mM sodium pyrophosphate, supplemented with protease inhibitor cocktail). Protein concentration was measured with a modified Bradford assay (Bio-Rad, Mississauga, Ontario, Canada). Total lysates and were separated by SDS–PAGE and transferred onto nitrocellulose filters (Bio-Rad). Blots were then probed with the indicated antibodies and developed using the enhanced chemiluminescence method.

siRNA transfection

Two siRNAs designed according to the XB130 gene sequence were used in this study, as previously described (Lodyga et al., 2009): XB130_A 5′-GATTCTT-GACCAGGAGAAC-3′, and XB130_B 5′CTACGAGTCCTACGATGAA-3′. The siSTABLE V2 non-targeting siRNA#1 from Dharmacon (Lafayette, CO) was used as a negative control. Oligonucleotides were delivered using the Oligofectamine reagent according to the manufacturer's specifications (Invitrogen).

Cell-spreading assay

TPC1 cells that were treated with either control siRNA or siRNA to knock down XB130 (A+B) for 48 hours were suspended with trypsin, neutralized with soybean trypsin inhibitor, centrifuged and resuspended in 5% FBS containing medium, and replated onto glass coverslips at a density of 17,000 cells/cm^2. Coverslips were washed twice with PBS, fixed in 4% paraformaldehyde at 15, 20, 25, 30, 40 minutes and mounted onto glass slides. Cell attachment to coverslips was essentially complete in 15 minutes. To quantify cell spreading, DIC images were taken using a 40× objective. The area occupied by each individual was determined by tracing the cell contour, followed by area measurement using the Image J software. Three independent experiments were conducted and in each 20-25 randomly selected fields were photographed to obtain a total of more than 150 cells in each group.

Wounding assay

TPC1 treated with either control siRNA or siRNA to knock down XB130 were harvested 48 hours after transfection using trypsin-EDTA and centrifuged at 800 ***g*** for 5 minutes. Equal cell numbers (6×10^5cells/well) were then plated on glass coverslips marked with a reference line through the middle of the coverslip. TPC1 cells were 80–90% confluent when they were wounded by dragging a plastic pipette tip across the cell surface (three wounds per coverslip, three coverslips per group). Cells were then incubated in medium supplemented with 20% FBS. Phase-contrast images of the wounds were recorded at 0, 6 and 12 hours above and below the reference line so that pictures were taken from the same wounded area. The wound closure was evaluated using ImageJ software by measuring the width of the remaining wound. Averages obtained are representative of three independent experiments.

Microscopy and immunofluorescence analysis

For immunofluorescence staining, cells were grown on glass coverslips. MTLn3 cells were plated on rat-tail type 1 collagen-coated coverslips. Following treatment cells were rapidly fixed by 4% paraformaldehyde for 30 minutes and washed with PBS. After quenching the paraformaldehyde with 100 mM glycine in PBS, the cells were permeabilized with 0.1% Triton-X-100 in 1% (w/v) albumin for 20 minutes and blocked with 3% (w/v) albumin for 1 hour. The coverslips were then incubated with primary antibodies for 1 hour, followed by washing and incubation with secondary antibodies for 1 hour. In certain cases the samples were also stained for actin with Rhodamine–phalloidin or Alexa-Fluor-350–phalloidin for 20 minutes. Coverslips were washed with PBS and mounted on glass slides using fluorescence mounting medium (Dako, Mississauga, Ontario, Canada). The staining was visualized using an Olympus IX81 microscope (Mellville, NY) coupled to an Evolution QEi Monochrome camera controlled by the QED inVivo Imaging software (Media Cybernetics, Bethesda, MD). For fluorescence quantification, all digital images were imported in ImageJ software (Abramoff et al., 2004). Translocation of XB130–GFP proteins to the lamellipodia (or the cell periphery) was evaluated by two methods: first, two observers independently scored >100 cells for each group in three separate experiments for the presence or absence of lamellipodial XB130. Second, the normalized peripheral signal intensity was determined for WT or mutant XB130–GFP proteins. To assess accumulation in the lamellipodium, first the lamellipodium per se was identified by Rhodamine–phalloidin staining. Subsequently, a line was drawn perpendicular to the lamellipodium and the distribution of XB130–GFP fluorescence intensity was determined along this line using ImageJ software. The peak value in the lamellipodium was divided by the minimal value obtained in the lamella, i.e. the area directly behind the lamellipodium. For each cell, four such lines were drawn and the obtained lamellipodium to lamella intensity ratios were averaged. In case of unstimulated cells (e.g. without EGF exposure), when no lamellipodium was formed, XB130–GFP intensity was measured at the cell periphery at two sites located within 2–3 and 5–6 μm from the plasma membrane, along a line perpendicular to the cell edge. These distances correspond to typical location of the lamellipodium and the lamella, respectively, in stimulated cells. Again four such ratios were determined and averaged. Finally the ratios obtained in stimulated cells were normalized to the average ratio in non-stimulated cells. Live imaging was done using an Olympus IX81 microscope (60× objective, Mellville, NY). Images were processed by the ImagePro Plus 3DS 5.1 software (Media Cybernetics). Images were collected every 20 seconds for 15 minutes.

Journal of Cell Science

Matrigel invasion

In vitro invasion through Matrigel was assayed using a Transwell-based cell culture chamber systems (Millipore-Chemicon, Temecula, CA). TPC1 cells treated with control siRNA or siRNA to knock down XB130 were harvested 48 hours after transfection using trypsin-EDTA and centrifuged at 800 ***g*** for 5 minutes. The cells were then counted and diluted to (1.2×10^5 cells/filter) in DMEM supplemented with 0.1% FBS. The cell suspension was added to the upper chamber of a polycarbonate membrane filter of 8 μM pore size containing rehydrated Matrigel layer. The lower chamber was filled with DMEM supplemented with 10% FBS. Cells were also seeded for a viability assay in adjacent wells, which did not contain a Transwell filter. Plates were incubated at 37°C for 24 hours. Cells remaining on the upper side of the filter and Matrigel were removed and the migrating cells on the lower side of the filter were stained with 0.1% Crystal Violet in 20% methanol for 20 minutes and allowed to air dry. Quantification of transmigrated cells was performed in three independent experiments (five inserts per group in total) using ten photographs per filter, on which stained nuclei were counted. Because we have previously shown that downregulation of XB130 can have effects on cell proliferation (Lodyga et al., 2009), we wished to ascertain that the observed reduction in transmigration was not merely due to compromised viability, and hence lower cells numbers. We therefore normalized the number of transmigrated cells according to the number of counted cells grown in parallel in separate six-well plate. The trypsinized cells were counted using a Coulter-counter (Beckman Coulter, Fullerton, CA).

Quantification of cells with lamellipodial protrusion

TPC1 cells treated with control siRNA or siRNA to knockdown XB130 (A+B) were harvested 24 hours after transfection and plated at 2×10^5 cells/well in a six-well plate as described earlier. Twenty-four hours after plating, cells were serum starved overnight in serum-free medium and treated with PMA (100 nM) for 30 or 60 minutes, then fixed, permeabilized, and stained with Rhodamine–phalloidin and Hoechst 33342 nuclear stain. Rhodamine–phalloidin and Hoechst fields were then merged and photographed (ten fields per group). Quantification of cells showing peripheral F-actin accumulation indicative of the lamellipodium was assessed in three independent experiments. Examples of positive and negative cells are shown in Fig. 12. The images were evaluated by two independent observers.

Statistical analysis

Statistical significance was determined by Student's *t*-test or one-way ANOVA (Tukey post-hoc testing) as appropriate, using GraphPad Prism 4.0 software.

We thank C. Di Ciano-Oliveira for help with the quantification of the lamellipodial translocation of the XB130 mutants. We thank K. Szaszi and A. Masszi for critical reading of the manuscript. This work was supported by grants to A.K. from the Canadian Institute of Health Research (CIHR, MOP-86535) the National Sciences and Engineering Research Council of Canada, and grants from CIHR to M.L. (MOP-13270, MOP-42546).

Supplementary material available online at
http://jcs.biologists.org/cgi/content/full/123/23/4156/DC1

References

Abramoff, M. D., Magelhaes, P. J. and Ram, S. J. (2004). Image processing with ImageJ. *Biophotonics Int.* **11**, 36-42.

Baumgartner, M., Sillman, A. L., Blackwood, E. M., Srivastava, J., Madson, N., Schilling, J. W., Wright, J. H. and Barber, D. L. (2006). The Nck-interacting kinase phosphorylates ERM proteins for formation of lamellipodium by growth factors. *Proc. Natl. Acad. Sci. USA* **103**, 13391-13396.

Benard, V., Bohl, B. P. and Bokoch, G. M. (1999). Characterization of rac and cdc42 activation in chemoattractant-stimulated human neutrophils using a novel assay for active GTPases. *J. Biol. Chem.* **274**, 13198-13204.

Bubb, M. R., Spector, I., Beyer, B. B. and Fosen, K. M. (2000). Effects of jasplakinolide on the kinetics of actin polymerization. An explanation for certain in vivo observations. *J. Biol. Chem.* **275**, 5163-5170.

Castelo, L. and Jay, D. G. (1999). Radixin is involved in lamellipodial stability during nerve growth cone motility. *Mol. Biol. Cell* **10**, 1511-1520.

Chan, A. Y., Raft, S., Bailly, M., Wyckoff, J. B., Segall, J. E. and Condeelis, J. S. (1998). EGF stimulates an increase in actin nucleation and filament number at the leading edge of the lamellipod in mammary adenocarcinoma cells. *J. Cell Sci.* **111**, 199-211.

Chan, A. Y., Bailly, M., Zebda, N., Segall, J. E. and Condeelis, J. S. (2000). Role of cofilin in epidermal growth factor-stimulated actin polymerization and lamellipod protrusion. *J. Cell Biol.* **148**, 531-542.

Chong, L. D., Traynor-Kaplan, A., Bokoch, G. M. and Schwartz, M. A. (1994). The small GTP-binding protein Rho regulates a phosphatidylinositol 4-phosphate 5-kinase in mammalian cells. *Cell* **79**, 507-513.

DePasquale, J. A. and Izzard, C. S. (1991). Accumulation of talin in nodes at the edge of the lamellipodium and separate incorporation into adhesion plaques at focal contacts in fibroblasts. *J. Cell Biol.* **113**, 1351-1359.

Dorfleutner, A., Stehlik, C., Zhang, J., Gallick, G. E. and Flynn, D. C. (2007). AFAP-110 is required for actin stress fiber formation and cell adhesion in MDA-MB-231 breast cancer cells. *J. Cell. Physiol.* **213**, 740-749.

Emaduddin, M., Edelmann, M. J., Kessler, B. M. and Feller, S. M. (2008). Odin (ANKS1A) is a Src family kinase target in colorectal cancer cells. *Cell Commun. Signal.* **6**, 7.

Etienne-Manneville, S. and Hall, A. (2002). Rho GTPases in cell biology. *Nature* **420**, 629-635.

Fan, L., Di Ciano-Oliveira, C., Weed, S. A., Craig, A. W., Greer, P. A., Rotstein, O. D. and Kapus, A. (2004). Actin depolymerization-induced tyrosine phosphorylation of cortactin: the role of Fer kinase. *Biochem. J.* **380**, 581-591.

Flynn, D. C., Leu, T. H., Reynolds, A. B. and Parsons, J. T. (1993). Identification and sequence analysis of cDNAs encoding a 110-kilodalton actin filament-associated pp60src substrate. *Mol. Cell. Biol.* **13**, 7892-7900.

Fukuda, T., Kiuchi, K. and Takahashi, M. (2002). Novel mechanism of regulation of Rac activity and lamellipodia formation by RET tyrosine kinase. *J. Biol. Chem.* **277**, 19114-19121.

Gatesman, A., Walker, V. G., Baisden, J. M., Weed, S. A. and Flynn, D. C. (2004). Protein kinase Calpha activates c-Src and induces podosome formation via AFAP-110. *Mol. Cell. Biol.* **24**, 7578-7597.

Han, B., Bai, X. H., Lodyga, M., Xu, J., Yang, B. B., Keshavjee, S., Post, M. and Liu, M. (2004). Conversion of mechanical force into biochemical signaling. *J. Biol. Chem.* **279**, 54793-54801.

Han, B., Lodyga, M. and Liu, M. (2005). Ventilator-induced lung injury: role of protein-protein interaction in mechanosensation. *Proc. Am. Thorac. Soc.* **2**, 181-187.

Haslam, R. J., Koide, H. B. and Hemmings, B. A. (1993). Pleckstrin domain homology. *Nature* **363**, 309-310.

Huveneers, S. and Danen, E. H. (2009). Adhesion signaling-crosstalk between integrins, Src and Rho. *J. Cell Sci.* **122**, 1059-1069.

Ichetovkin, I., Grant, W. and Condeelis, J. (2002). Cofilin produces newly polymerized actin filaments that are preferred for dendritic nucleation by the Arp2/3 complex. *Curr. Biol.* **12**, 79-84.

Keely, P. J., Westwick, J. K., Whitehead, I. P., Der, C. J. and Parise, L. V. (1997). Cdc42 and Rac1 induce integrin-mediated cell motility and invasiveness through PI(3)K. *Nature* **390**, 632-636.

Lodyga, M., Bai, X. H., Mourgeon, E., Han, B., Keshavjee, S. and Liu, M. (2002). Molecular cloning of actin filament-associated protein: a putative adaptor in stretch-induced Src activation. *Am. J. Physiol. Lung Cell. Mol. Physiol.* **283**, L265-L274.

Lodyga, M., De Falco, V., Bai, X. H., Kapus, A., Melillo, R. M., Santoro, M. and Liu, M. (2009). XB130, a tissue-specific adaptor protein that couples the RET/PTC oncogenic kinase to PI 3-kinase pathway. *Oncogene* **28**, 937-949.

MacLean-Fletcher, S. and Pollard, T. D. (1980). Mechanism of action of cytochalasin B on actin. *Cell* **20**, 329-341.

Matsui, T., Maeda, M., Doi, Y., Yonemura, S., Amano, M., Kaibuchi, K., Tsukita, S. and Tsukita, S. (1998). Rho-kinase phosphorylates COOH-terminal threonines of ezrin/radixin/moesin (ERM) proteins and regulates their head-to-tail association. *J. Cell Biol.* **140**, 647-657.

Mouneimne, G., Soon, L., DesMarais, V., Sidani, M., Song, X., Yip, S. C., Ghosh, M., Eddy, R., Backer, J. M. and Condeelis, J. (2004). Phospholipase C and cofilin are required for carcinoma cell directionality in response to EGF stimulation. *J. Cell Biol.* **166**, 697-708.

Nobes, C. D. and Hall, A. (1995). Rho, rac, and cdc42 GTPases regulate the assembly of multimolecular focal complexes associated with actin stress fibers, lamellipodia, and filopodia. *Cell* **81**, 53-62.

Qian, Y., Baisden, J. M., Zot, H. G., Van Winkle, W. B. and Flynn, D. C. (2000). The carboxy terminus of AFAP-110 modulates direct interactions with actin filaments and regulates its ability to alter actin filament integrity and induce lamellipodia formation. *Exp. Cell Res.* **255**, 102-113.

Segall, J. E., Tyerech, S., Boselli, L., Masseling, S., Helft, J., Chan, A., Jones, J. and Condeelis, J. (1996). EGF stimulates lamellipod extension in metastatic mammary adenocarcinoma cells by an actin-dependent mechanism. *Clin. Exp. Metastasis* **14**, 61-72.

Smith, A., Carrasco, Y. R., Stanley, P., Kieffer, N., Batista, F. D. and Hogg, N. (2005). A talin-dependent LFA-1 focal zone is formed by rapidly migrating T lymphocytes. *J. Cell Biol.* **170**, 141-151.

Subauste, M. C., Von Herrath, M., Benard, V., Chamberlain, C. E., Chuang, T. H., Chu, K., Bokoch, G. M. and Hahn, K. M. (2000). Rho family proteins modulate rapid apoptosis induced by cytotoxic T lymphocytes and Fas. *J. Biol. Chem.* **275**, 9725-9733.

Takaishi, K., Sasaki, T., Kato, M., Yamochi, W., Kuroda, S., Nakamura, T., Takeichi, M. and Takai, Y. (1994). Involvement of Rho p21 small GTP-binding protein and its regulator in the HGF-induced cell motility. *Oncogene* **9**, 273-279.

Taunton, J., Rowning, B. A., Coughlin, M. L., Wu, M., Moon, R. T., Mitchison, T. J. and Larabell, C. A. (2000). Actin-dependent propulsion of endosomes and lysosomes by recruitment of N-WASP. *J. Cell Biol.* **148**, 519-530.

Taylor, J. M., Richardson, A. and Parsons, J. T. (1998). Modular domains of focal adhesion-associated proteins. *Curr. Top. Microbiol. Immunol.* **228**, 135-163.

Tominaga, T., Sahai, E., Chardin, P., McCormick, F., Courtneidge, S. A. and Alberts, A. S. (2000). Diaphanous-related formins bridge Rho GTPase and Src tyrosine kinase signaling. *Mol. Cell* **5**, 13-25.

Turunen, O., Wahlstrom, T. and Vaheri, A. (1994). Ezrin has a COOH-terminal actin-binding site that is conserved in the ezrin protein family. *J. Cell Biol.* **126**, 1445-1453.

Weed, S. A., Du, Y. and Parsons, J. T. (1998). Translocation of cortactin to the cell periphery is mediated by the small GTPase Rac1. *J. Cell Sci.* **111**, 2433-2443.

Weiner, O. D., Neilsen, P. O., Prestwich, G. D., Kirschner, M. W., Cantley, L. C. and Bourne, H. R. (2002). A PtdInsP(3)- and Rho GTPase-mediated positive feedback loop regulates neutrophil polarity. *Nat. Cell Biol.* **4**, 509-513.

Xu, J., Bai, X. H., Lodyga, M., Han, B., Xiao, H., Keshavjee, S., Hu, J., Zhang, H., Yang, B. B. and Liu, M. (2007). XB130, a novel adaptor protein for signal transduction. *J. Biol. Chem.* **282**, 16401-16412.

Yip, S. C., El-Sibai, M., Hill, K. M., Wu, H., Fu, Z., Condeelis, J. S. and Backer, J. M. (2004). Over-expression of the p110beta but not p110alpha isoform of PI 3-kinase inhibits motility in breast cancer cells. *Cell Motil. Cytoskeleton* **59**, 180-188.

Zhang, J., Park, S. I., Artime, M. C., Summy, J. M., Shah, A. N., Bomser, J. A., Dorfleutner, A., Flynn, D. C. and Gallick, G. E. (2007). AFAP-110 is overexpressed in prostate cancer and contributes to tumorigenic growth by regulating focal contacts. *J. Clin. Invest.* **117**, 2962-2973.

Zhang, S., Han, J., Sells, M. A., Chernoff, J., Knaus, U. G., Ulevitch, R. J. and Bokoch, G. M. (1995). Rho family GTPases regulate p38 mitogen-activated protein kinase through the downstream mediator Pak1. *J. Biol. Chem.* **270**, 23934-23936.

Journal of Cell Science